Materials Today Energy 39 (2024) 101467

Contents lists available at ScienceDirect

Materials Today Energy

journal homepage: www.journals.elsevier.com/materials-today-energy/

New promising class of anode materials for Ca-ion battery: polyaromatic hydrocarbons

Alexey P. Maltsev [a, c, *], Ilya V. Chepkasov [a, b, c, **], Artem R. Oganov [a, ***]

[a] Skolkovo Institute of Science and Technology, Bolshoy Boulevard 30, bld. 1, Moscow, 121205, Russian Federation
[b] Katanov Khakas State University, 90 Lenin pr., 655017, Abakan, Russian Federation

ARTICLE INFO

Article history:
Received 19 September 2023
Received in revised form
11 November 2023
Accepted 30 November 2023
Available online 7 December 2023

Keywords:
Ab inito
Calcium
DFT
Ion batteries
Electrode

ABSTRACT

Using first-principles calculations we propose new anode materials for calcium-ion batteries, namely anthracene (AN), tetracene (TN) and pentacene (PN) crystals. We show that adsorption of calcium atoms on isolated AN, TN and PN molecules is energetically favorable, as well as intercalation into bulk crystals in a wide range of calcium concentrations. For all crystals, volume expansion during intercalation is less than 20% and for pentacene, it is less than 8%. We assess the diffusion and electronic properties of AN, TN and PN. We show that calcium diffusion barriers along the polyacene molecules are less than 0.45 eV, but calcium diffusion is limited by "jumps" between the molecules. Sequential band filling upon increasing levels of intercalation leads to the reentrant semiconducting-metallic-semiconducting behavior. Our results point to the promise of anthracene, tetracene, and pentacene as anodes for calcium-ion batteries.

1. Introduction

Ca-ion batteries (CIB) have received increased interest in recent years due to their advantages such as natural abundance and low cost of calcium, chemical safety, and high capacity [1–5]. They also have the advantage that the divalent ion Ca^{2+} carries twice as much charge as monovalent ions such as Li^{+} and Na^{+} which contributes to greater capacitance at the same concentration. Among all divalent ions, Ca^{2+} is the most promising one due to its low potential −2.87 V versus the standard hydrogen electrode (SHE), which is close to that of Li^{+} (−3.04 V) [6,7]. Various materials have been considered as anodes for such batteries; in particular, calcium metal anode is considered promising, but this technology is very complex and faces certain limitations [8,9], moreover in nonaqueous electrolytes, it forms a strong passivation layer that inhibits electron transfer through the anode/electrolyte interphase [10,11]. Calcium alloys are considered an alternative to metal calcium anodes because they often have both high specific capacitance and low potential [5,12]. Despite these advantages, such anodes have a significant drawback associated with the very high volume changes up to 3–4 times [1,13]. Another option for anode material is intercalation materials [14–17]. Graphite is the most typical and best studied material for metal-ion battery technology. Calcium intercalation into graphite leads to the CaC_6 crystal structure, with its unique rhombohedral, $R\bar{3}\,m$ space group compared to other MC_6 compounds with hexagonal symmetry [18]. Borophene and hydrogenated defective graphene have been investigated by DFT and shown to be suitable as materials for calcium battery anodes with specific capacities of 800 and 591 mAh/g, respectively [19,20].

Polyaromatic hydrocarbons (PAH), such as benzene, naphthalene, anthracene, and tetracene, are also promising anode materials [21–23]. These PAH are considered prototypical carbonaceous materials, which mimic sp^2 allotropic forms of carbon such as graphene, graphite, carbon nanotubes, etc. Molecules inside polyacene crystals are bonded together by van der Waals dispersion forces, and crystals are compliant with the insertion of intercalants. Studies of the adsorption of lithium atoms on polyaromatic hydrocarbons showed the promise of these materials for lithium-ion batteries [24–27]. Using semi-quantitative methods, Friedlein et al. [28] compared the charge storage capability of PAH and showed that small and medium-size PAH might have the highest energy storage ability among all pure-carbon systems.

* Corresponding author.
** Corresponding author.
*** Corresponding author.
E-mail addresses: alexey.maltsev@skoltech.ru (A.P. Maltsev), I.Chepkasov@skoltech.ru (I.V. Chepkasov), a.oganov@skoltech.ru (A.R. Oganov).
[c] Contributed equally to this work.

https://doi.org/10.1016/j.mtener.2023.101467
2468-6069/

Table 1
Lattice parameters of polyacene crystals.

Polyacenes	*a*, Å	*b*, Å	*c*, Å	*α*, °	*β*, °	*γ*, °	*Vol*, Å^3
AN (Exp.) [38]	8.55	6.01	11.17	90	124.59	90	473.16
TN (Exp.) [39]	6.05	7.83	13.01	77.12	72.11	85.79	572.97
PN (Exp.) [39]	6.27	7.71	14.44	76.75	88.01	84.52	677.32
AN (our calc.)	8.39	5.86	11.05	90	125.24	90	444.04
TN (our calc.)	6.03	7.32	12.62	78.71	73.05	85.57	523.17
PN (our calc.)	6.27	7.55	14.18	77.65	88.83	83.93	652.17

AN, anthracene; TN, tetracene; PN, pentacene.

In order to evaluate the prospects of these materials as anodes of Ca-ion batteries, in this work we have considered the intercalation of Ca with polyaromatic hydrocarbon (PAH) crystals such as anthracene (AN), tetracene (TN), and pentacene (PN).

2. Computational methodology

All density functional theory (DFT) calculations were carried out using the VASP code [29,30]. After the convergence test, an energy cutoff of 400 eV was used for the calculations. The Brillouin zones of the primitive cells of polyacenes with calcium atoms were sampled using 4 × 4 × 4 gamma-centered k-point meshes [31]. For electronic density of states (DOS) calculations, the k-point grid was increased to 8 × 8 × 8, the tetrahedron method with Blöchl corrections was used. For the calculations of the isolated molecules, the maximum force on each atom was set to be less than 0.01 eV/Å for the optimized configurations. The thresholds of electronic and ionic self-consistency were set to 10^{-6} and 10^{-7} eV, respectively. Gaussian smearing with $\sigma = 0.05$ eV was used. We used the DFT-D3 method of Grimme [32,33], known to have good overall performance for molecular crystals. The obtained lattice parameters of PAH with the DFT-D3 method of Grimme are in good agreement with experimental data (Table 1). Electron transfer was explored using Bader analysis [34]. DOS and band structures were analyzed using the Pymatgen package [35]. The atomic structures were illustrated using the VESTA package [36]. Using the climbing image nudged elastic band (CI-NEB) [37] approach, we assessed diffusion barriers for the Ca atom in PAH crystals. Diffusion paths consisted of seven images. Diffusion barriers were calculated in the 2 × 2 × 2 PAH supercells with 385, 481, and 577 atoms for AN, TN, and PN, respectively.

To estimate the energetics directly related to the stability of different configurations, we calculated the intercalation energy E_i per Ca atom, which corresponds to the energy change when n_{Ca} Ca atoms are moved from the bulk Ca crystal into the polyacene crystal, defined as

$$E_i = [E(Ca_nPAH) - E(PAH)]/n_{Ca} - E(Ca), \quad (1)$$

where $E(Ca_nPAH)$ is the total energy of the Ca-intercalated polyacene system, $E(PAH)$ is the energy of the pristine polyacene, and $E(Ca)$ - is the total energy of the Ca atom in its bulk structure. The number of atoms n is a multiple of 0.5 because there are two PAH molecules in the unit cell.

The thermodynamic phase stability of the systems was also assessed by the phase diagrams in (enthalpy of formation-composition) coordinates (convex hulls). From the DFT energies of pseudo-binary phase Ca_xPAH_{1-x} with Ca and PAH compositional blocks, we have calculated the enthalpy of formation per block:

$$E_f \Big/ block = E(Ca_xPAH_{1-x}) - xE(Ca) - (1-x)E(PAH), \quad (2)$$

where $E(Ca_xPAH_{1-x})$ is the total energy of the Ca-intercalated polyacene system.

A convex hull was constructed between the points (x, $E_f/block$) = (0, 0) and (1, 0). Lines connect structures with the lowest energy so that they form a convex hull. Structures that lie on the convex hull are thermodynamically stable, and structures above the convex hull are metastable (their decomposition energies are positive).

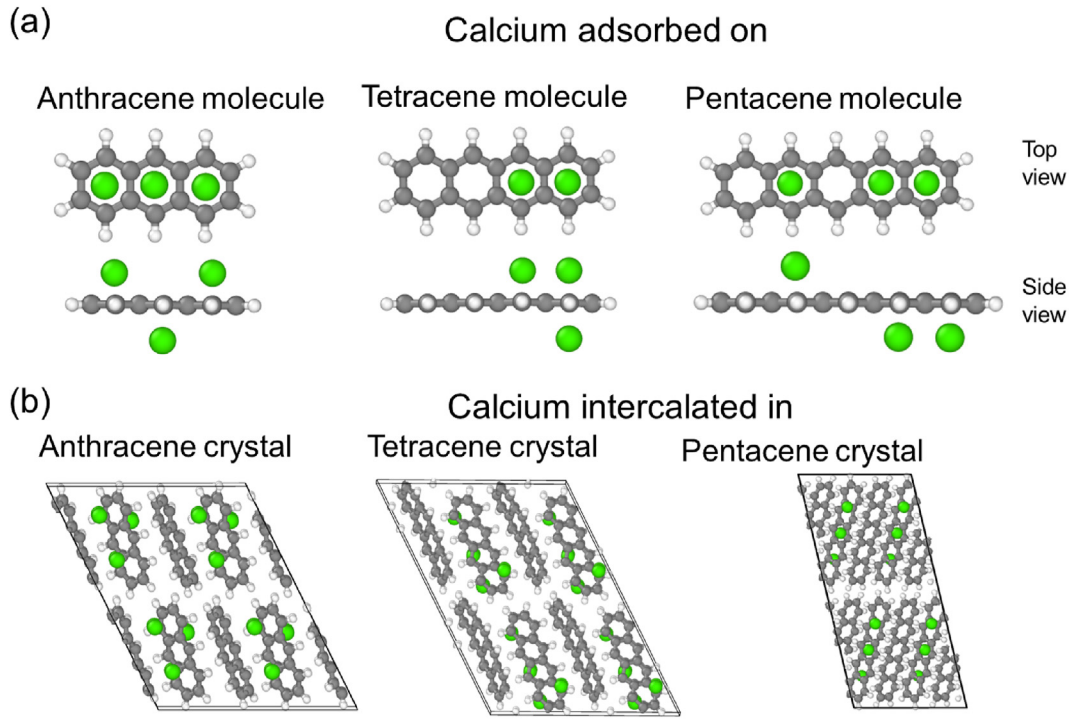

Fig. 1. (a) Schematic representation of AN, TN, and PN molecules with adsorbed Ca atoms. (b) Schematic representation of anthracene, pentacene, and tetracene crystals (2 × 2 × 2 supercells) with intecalated Ca atoms. AN, anthracene; TN, tetracene; PN, pentacene.

The concentration x of Ca atoms in PAH is defined as follows:

$$x = \frac{n(Ca)}{n(Ca) + n(PAH)}, \quad (3)$$

and the number of calcium atoms n is the number of atoms per formula unit of the polyacene molecule (there are two molecules in the unit cell).

The average voltages for the thermodynamically stable structures were calculated from DFT total energies. For two phases on a convex hull, $Ca_{n_1}PAH$ and $Ca_{n_2}PAH$ ($n_2 > n_1$), the following reaction is assumed to occur:

$$Ca_{n_1}PAH + (n_2 - n_1)Ca \rightarrow Ca_{n_2}PAH \quad (4)$$

The voltage, V, is calculated by the following formula:

$$V = -\frac{\Delta G}{z(n_2 - n_1)} \approx -\frac{\Delta E}{z(n_2 - n_1)} = -\frac{E(Ca_{n_2}PAH) - E(Ca_{n_1}PAH)}{z(n_2 - n_1)} + \frac{E(Ca)}{z} \quad (5)$$

where the Gibbs free energy is approximated by the internal energy, as pV and thermal energy are assumed to be small, and $z = 2$ is the formal charge of the calcium ion.

The theoretical capacity of the AN, TN, and PN crystals with different amounts of calcium was calculated using Faraday's law:

$$Capacity = \frac{\nu \cdot z \cdot F}{3.6 \cdot M} \quad (6)$$

where ν is the number of Ca atoms per polyacene molecule, $F = 96{,}485$ C/mol, Faraday constant, and M - molar mass of the polyacene molecule.

3. Results and discussion

3.1. Isolated molecules of polyaromatic hydrocarbons

To study Ca intercalation in anthracene, tetracene, and pentacene crystals, in the first step we studied the adsorption of Ca atoms on isolated PAH molecules (1 – 6 Ca atoms for anthracene molecule, 1 – 8 Ca atoms for tetracene molecule, and 1 – 10 Ca atoms for pentacene molecule) (see Fig. 1). Different sites (22, 68, and 263 structures for anthracene, tetracene, and pentacene molecules, respectively) for adsorption were considered. Fig. 2a, b, and c show all optimized ground states of anthracene-Ca, tetracene-Ca, and pentacene-Ca complexes with numbers of Ca atoms from 1 to 6, 8, and 10, respectively. For all considered polyacenes, it was found that Ca-polyacene complexes are thermodynamically stable even with a high number of Ca atoms, with absorption

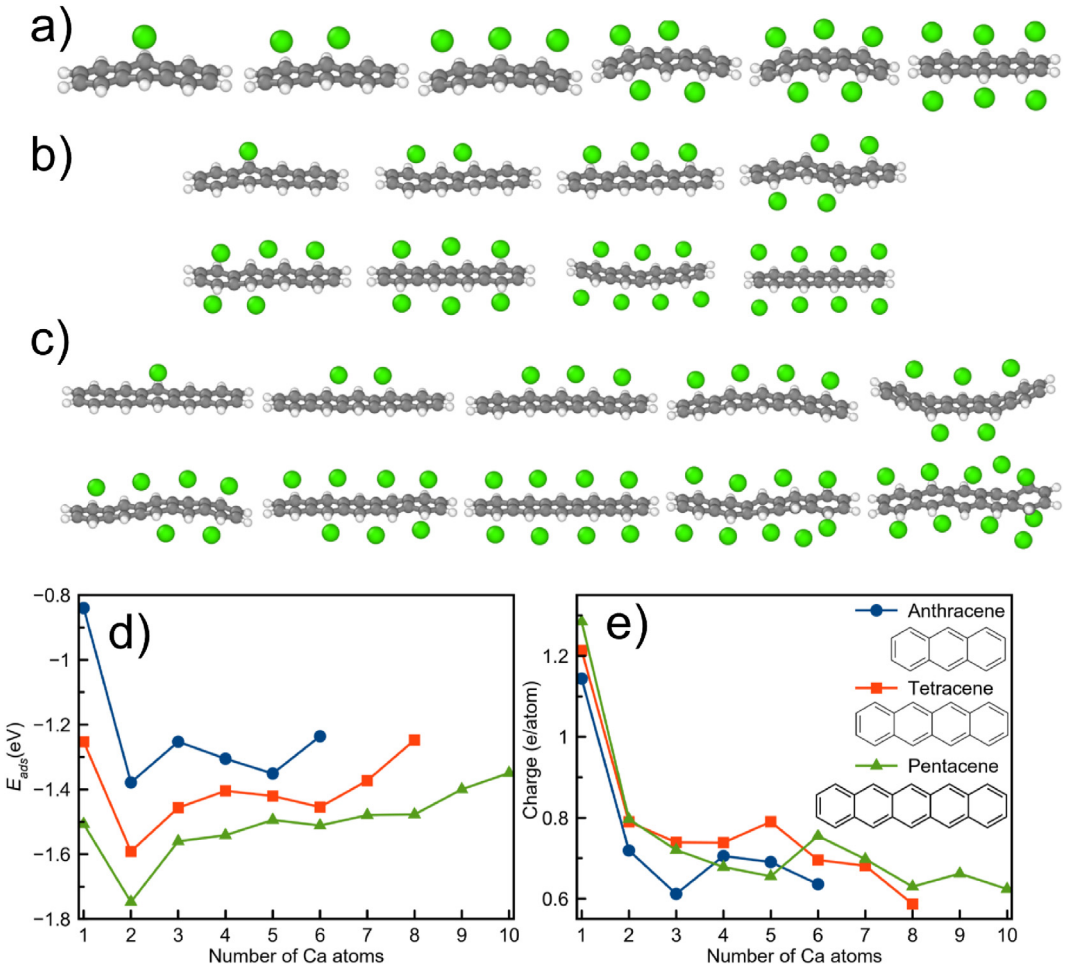

Fig. 2. Optimized geometries of polyacene molecules with adsorbed Ca atoms: (a) anthracene, (b) tetracene, and (c) pentacene molecules. (d) Energy required to take a Ca atom from the bulk crystal and adsorb it on free-standing polyacene molecules, and (e) charge transfer from Ca atoms to polyacene molecules as a function of the number of adsorbed atoms.

energies $E_{abs} = 1.2 - 1.7$ eV (Fig. 2d). One Ca atom while adsorbed tends to occupy a position above the central benzene ring (or one of the central rings of tetracene), while adsorption on the peripheral benzene ring is less energetically favorable by about 0.2-0.4 eV.

When the number of calcium atoms increases from 1 to 3, the atoms have a tendency to occupy the same side of the polyacene molecule (Fig. 2). However, when 4 calcium atoms are present (in the case of anthracene and tetracene) or 5 calcium atoms are present (in the case of pentacene), adsorption on the opposite side becomes more favorable. As the calcium concentration increases, the atoms no longer occupy the positions directly above the benzene rings or the C–C faces of the benzene ring; instead, they are distributed uniformly along the polyacene molecule. The distances from the calcium atom to the nearest benzene ring also increase with an increase in calcium concentration. In the case of the central benzene rings, the distance increases from 2.15 Å to 2.21 – 2.23 Å. In the case of the peripheral rings, the distance increases to 2.35 – 2.42 Å. Overall, the calcium atoms tend to adsorb along the polyacene molecules, with the exception of pentacene with 9 and 10 calciums, where some atoms are adsorbed on the sides of the molecule due to their steric repulsion.

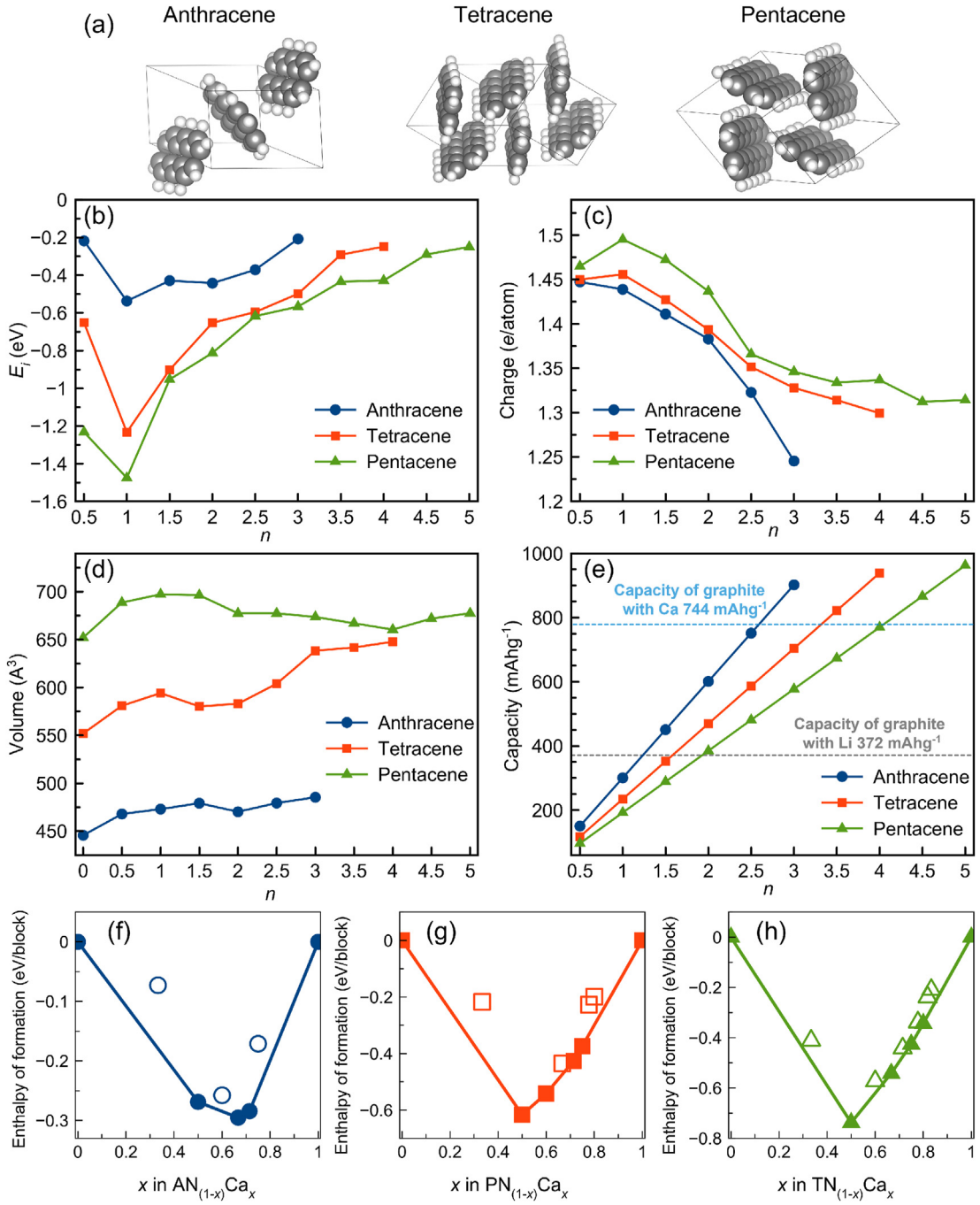

Fig. 3. Characteristics of Ca intercalations in PAH crystals as a function of the number of Ca atoms *n* intercalated in the PAH crystal. (a) View of anthracene, tetracene, and pentacene crystals. (b) Intercalation energy. (c) Charge transfer from Ca atoms to PAH crystals. (d) Change of the volume of PAH crystal. (e) Capacity of the PAH crystals with intercalated Ca atoms. (f–h) Calculated convex hulls of the crystalline AN-Ca (f), TN-Ca (g), and PN-Ca (h) systems with respect to pristine crystalline polyacenes and crystalline Ca. PAH, polyaromatic hydrocarbons.

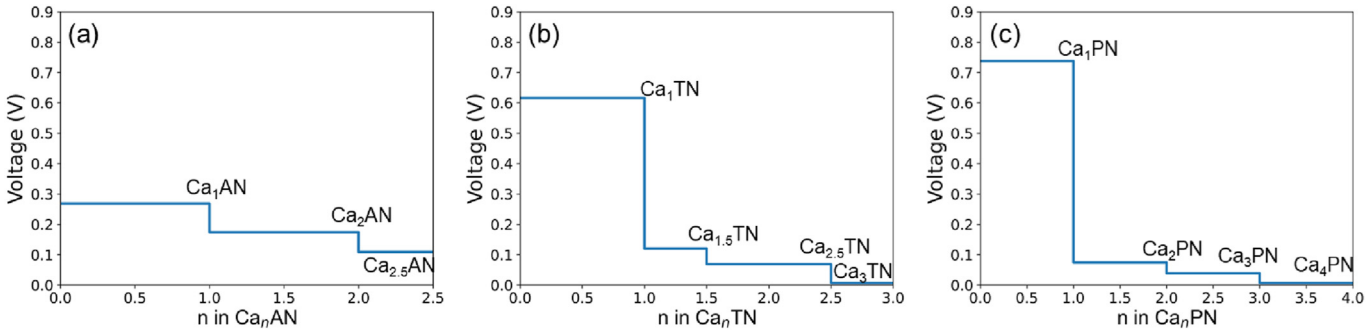

Fig. 4. Calculated average voltages relative to calcium metal for AN-Ca (a), TN-Ca (b), PN-Ca (c) structures on the convex hull (Fig. 3(f–e)). AN, anthracene; TN, tetracene; PN, pentacene.

The calculated Bader charges (Fig. 2e) [34] show that with increasing concentrations of Ca, the number of electrons that each atom donates to the PAH molecules changes from 1.15 e^- to 0.6 e^-. The adsorption of the first two calcium atoms in all three cases is the most energetically favorable process (Fig. 2d), while the adsorption energy of the subsequent calcium atoms decreases with increasing Ca concentration. This is in accordance with Bader analysis and electronic density of states calculations: Bader charge of the calcium atom has a maximum at $n = 1$.

3.2. Polyaromatic hydrocarbons crystals

After investigating the bonding between Ca atoms and individual PAH molecules, we conducted simulations to model the incorporation of Ca atoms into bulk PAH crystals Fig. 3a. Ca atoms were added to the PAH cells at various positions, then structures were fully optimized, and structures with the lowest energies were considered.

The intercalation energy E_i calculated through Eq. (1) is presented in Fig. 3b. Fig. 3f-e shows the phase diagrams in the coordinates of the enthalpy of formation-composition (convex hull) (Eq. (2)). The values of E_i for all calculated structures are negative, but not all structures lie on the convex hull, indicating that some structures are metastable. The highest concentrations of calcium at which the structures are thermodynamically stable are $x = 0.71$ ($n = 2.5$), $x = 0.75$ ($n = 3$), and $x = 0.8$ ($n = 4$) for AN, TN, and PN, respectively (Fig. 3f-h). Intercalation energies are close to the binding energies of Li and Ca in bilayer graphene with AB-stacking

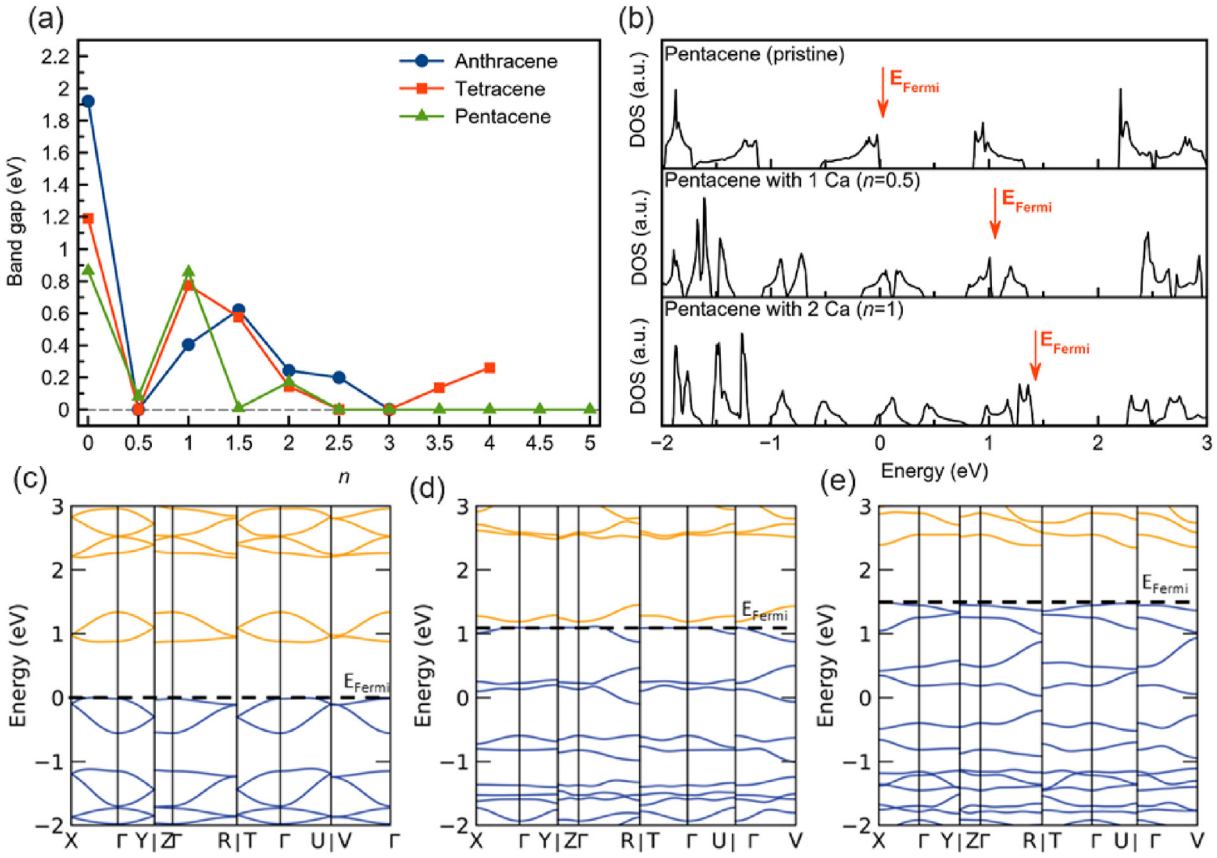

Fig. 5. (a) Band gaps of PAH of the number n of Ca atoms intercalated in PAH crystal. (b) Density of states of pristine pentacene crystal with 1 and 2 Ca atoms in the unit cell. (c–e) Band structures calculated for pristine pentacene (c), pentacene with 1 calcium atom (d), and pentacene with 2 calcium atoms (e). Dashed horizontal lines show Fermi levels aligned to show the relationship between these band structures and the effect of doping.

and approximately twice lower than the binding energies of Li and Ca in bilayer graphene with AA-stacking [40]. The minima of intercalation energy are observed at $x = 0.5$ ($n = 1$) for all PAH, indicating the first and second calcium atoms intercalate into polyacene unit cells much more easily than the subsequent ones. This result is in agreement with our calculations of the average voltages of structures (Fig. 4).

At $n = 1$ of Ca in Ca_nPAH, the average voltages are equal to 0.27 V, 0.62 V, and 0.74 V for AN, TN, and PN, respectively, while at $n > 1$, the average voltages of the structures for tetracene and pentacene exceed the potential of calcium metal by no more than 0.01 V. Low calcium insertion voltages at high concentrations indicate the possibility of high performance of polyacene molecules as anode materials.

Trends in intercalation energies are related to charge transfer from Ca atoms to the polyacene molecules, Fig. 3b. The intercalation energy maximum (1 Ca atoms per formula unit) is associated with the maximum charge donation from Ca atoms: 1.49 e^-, 1.46 e^- for PN and TN, respectively; for AN, crystal charges on one and two Ca atoms in the unit cell (0.5 and 1 atom per formula unit) are almost equal (1.45 and 1.44 e^-, respectively). As the concentration increases, the energy gain decreases monotonically, simultaneously with a decrease in charge transfer from Ca atoms from 1.45to 1.5 e^- to $\sim 1.25 - 1.3$ e^-.

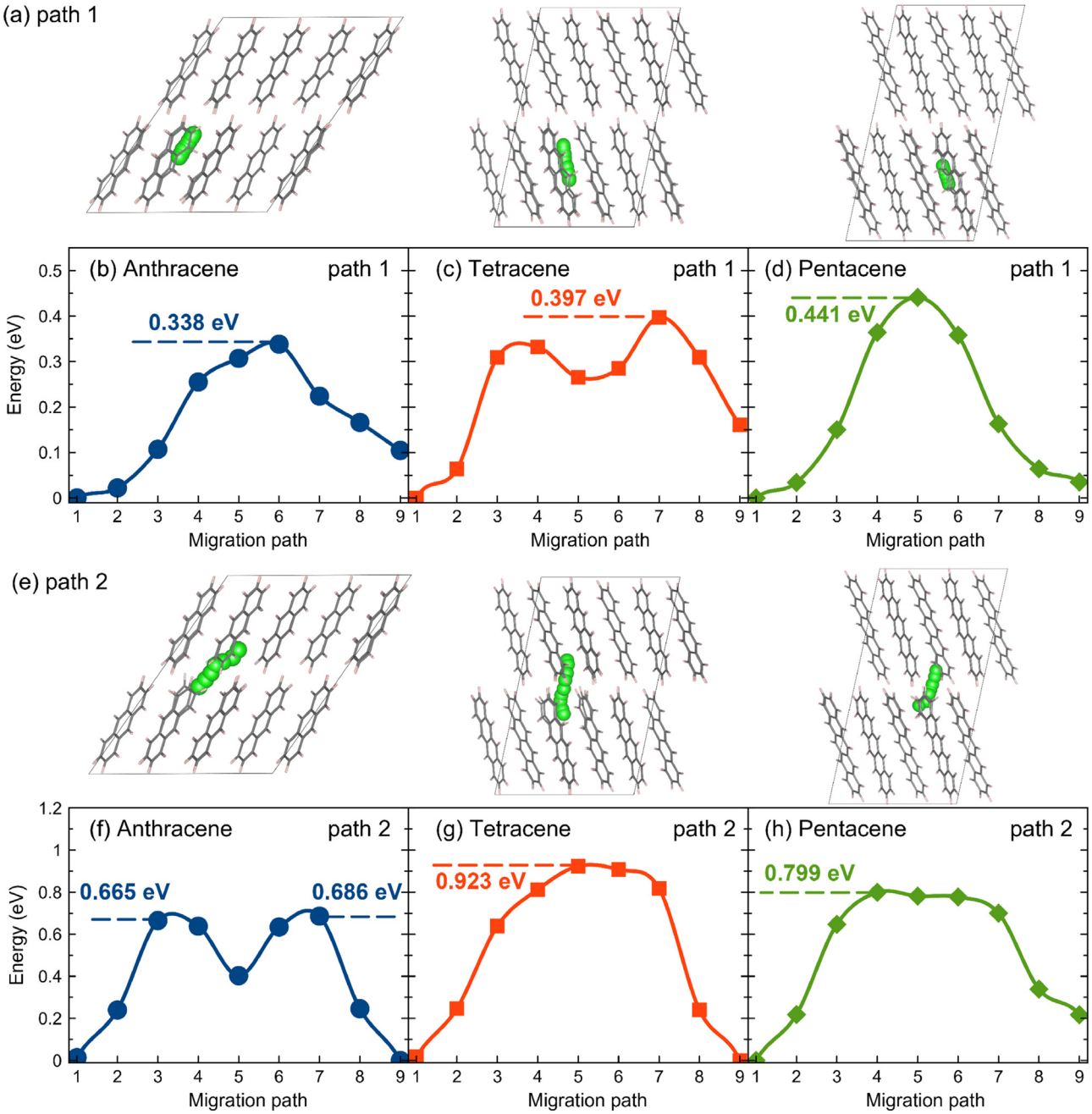

Fig. 6. (a) Diffusion paths of Ca along the molecules in PAH crystals. (b–d) Migration barrier of Ca along the molecules in PAH crystals. (e) Diffusion paths of Ca between the molecules in PAH crystals. (f–h) The barrier of Ca migration from one molecule to another in PAH crystals. PAH, polyaromatic hydrocarbons.

According to the calculations, the maximum volume expansion is 17% for the tetracene crystal and is lower than 10% for anthracene and pentacene. Volume as a function of concentration is shown in Fig. 3c. It can be seen that volume changes nonmonotonically. At a low concentrations of Ca ($x \sim 0.33 - 0.6$, $n \sim 0.5 - 1.5$), volume increases due to spatial repulsion of Ca atoms and polyacene molecules; after $x \sim 0.6 - 0.66$ volume slightly decreases due to an increase in total bonding between Ca and polyacenes; at high concentrations, saturation occurs: charge transfer from calcium atoms and energy gain decrease, spatial repulsion increases, and as a result, the volume of the crystal increases. It is important to note that in practice, volume change may also depend on the intercalation of electrolyte components, defects and solid electrolyte interface (SEI) formation, electrolyte compatibility, and amorphization upon cycling; however, these phenomena are beyond the scope of the current study.

At a concentration of Ca greater than $x = 0.6$ ($n = 1.5$) in anthracene and more than $x = 0.66$ ($n = 2$) in tetracene and pentacene, the theoretical capacity (calculated using formula 6) of calcium-intercalated polyacenes exceeds the theoretical capacity of lithium-intercalated graphite, which is the most popular anode material in ion batteries. It is notable, that these structures lie on the convex hull and are thermodynamically stable. At the maximum concentration at which the structures are thermodynamically stable ($x \sim 0.7 - 0.8 (n \sim 2.5 - 3.5)$), the theoretical capacity is approximately 2 times higher than that of lithium graphite. Compared to calcium in graphite, polyaromatic hydrocarbons show similar theoretical capacities.

Keeping in mind the possibility to tune the electronic structure of PAH crystals [41–43], we investigated the effects of intercalation on their electronic properties. Fig. 5a represents the band gaps of AN, TN, and PN as a function of Ca intercalation. We find the band gaps of AN, TN, and PN crystals to be 1.92 eV, 1.19 eV, and 0.85 eV, respectively, similar to previous DFT calculations and (as is normal for DFT band gaps) significantly lower (by $\sim 1 - 2$ eV) than experimental gaps [44].

Pristine polyacene crystals have two nearly degenerate low-energy conduction bands, separated by 1–1.5 eV from the higher bands (Fig. 5c). When one calcium atom is added to the unit cell, it donates two electrons, which fill the lowest of the two nearly-degenerate lowest-energy conduction bands (Fig. 5d), making the crystal a very narrow-gap (0.08 eV for pentacene) semiconductor or a metal (in the case of anthracene and tetracene). When the second Ca atom is added, another two electrons are added, which fill the second lowest conduction band (Fig. 5e), and the crystal gets a much wider band gap of 0.4, 0.77, and 0.86 eV for AN, TN, and PN, respectively. If more calcium atoms are intercalated, the system becomes again a narrow-gap semiconductor or metal, as illustrated in the example for pentacene in Fig. 5b. This result is in agreement with previous calculations of the electronic properties of alkali-intercalated tetracene [45].

Finally, to get insight into the intercalation kinetics, we also assessed the diffusion barriers for Ca in PAH. The intercalant atom diffusivity is an important factor governing the actual operation of the battery, as the charge/discharge of metal-ion batteries mainly depend on the diffusion of metal atoms in the anode materials. Using the CI-NEB [37] method, we calculated diffusion barriers for the Ca atom in PAH crystals between and along the PAH molecules. The diffusion paths are presented in Fig. 6 (a, e). The associated energy barriers are shown in Fig. 6 (b-d, f-h). The diffusion paths along the PAH molecules (path 1) show barriers from 0.34 eV to 0.44 eV (Fig. 6(b–d)), which are comparable or smaller than calcium diffusion barriers in other electrode materials, such as $Ca_xNa_{0.5}VPO_{4.8}F_{0.7}$ [46], $Ca_xCo_2O_4$ [47], α-V_2O_5 [48], Ca_xMoO_3 [49], and $CaMn_4O_8$ [50]. However, the diffusion is governed by the 'jumps' between the molecules. The diffusion barriers of 'jumps' are 0.68 eV for anthracene, 0.92 eV for tetracene, and 0.8 eV for pentacene. These values are still close to those of $Ca_xNa_{0.5}VPO_{4.8}F_{0.7}$ [46] and $Ca_xCo_2O_4$ [47] electrodes and significantly lower than those in α-V_2O_5 [48], Ca_xMoO_3 [49], and $CaMn_4O_8$ [50] materials.

High intercalation energies, low volume expansion, and satisfactory kinetic and electronic properties make polyacene molecules promising anode materials for calcium-ion batteries for mobile and stationary applications. Among the three PAHs considered, pentacene stands out for its lowest volumetric expansion and the most favorable electronic properties. The activation barrier for calcium 'jumps' in pentacene is lower than in tetracene, and the maximum theoretical capacity is at the same level as graphite. Therefore, we believe that among the three PAH anodes, pentacene is the most promising one.

4. Conclusions

With the use of DFT calculations, we studied the intercalation and diffusion of calcium atoms in anthracene (AN), tetracene (TN), and pentacene (PN) crystals. Up to 3, 4, and 5 calcium atoms per formula unit of the polyacene can be intercalated into AN, TN, and PN, respectively. Intermediates with Ca concentrations $x = 0.71$, 0.75, and 0.8 ($n = 2.5$, 3, and 4) in AN, TN, and PN, respectively, are thermodynamically stable. The calculated activation energies of calcium diffusion along the molecules are less than 0.45 eV, and the barriers of Ca-jumps between molecules are less than 0.95 eV, which serve as diffusion-limiting moves. During intercalation, several conduction bands can be filled, so systems exhibit reentrant metal-semiconductor behavior. For all crystals, the volume change during intercalation is less than 20%, and for pentacene, it is remarkably less than 8%.

Our results provide insights into the thermodynamics and kinetics of calcium intercalation into polyaromatic hydrocarbon crystals. Values of binding energy, satisfactory activation barriers of diffusion, and low volume expansion make polyacene crystals promising anode materials for calcium-ion batteries.

Credit author statement

Alexey P. Maltsev: Conceptualization, Methodology, Formal analysis, Investigation, Writing - Original Draft, Visualization.

Ilya V. Chepkasov: Conceptualization, Methodology, Formal analysis, Investigation, Writing - Original Draft, Visualization.

Artem R. Oganov: Supervision, Methodology, Writing - Review & Editing.

Declaration of competing interest

The authors declare that they have no known competing financial interests or personal relationships that could have appeared to influence the work reported in this paper.

Data availability

Data will be made available on request.

Acknowledgment

The authors are grateful to Arkady V. Krasheninnikov (HZDR) for the discussion. This work was supported by the Russian Science Foundation grant No. 19-72-30043. Calculations were carried out using the resources of the Center for Information and Computing of Novosibirsk State University and the Arkuda supercomputer of Skoltech.

References

[1] R.J. Gummow, G. Vamvounis, M.B. Kannan, Y. He, Calcium-ion batteries: current state-of-the-art and future perspectives, Adv. Mater. 30 (39) (2018) 1801702.

[2] A.L. Lipson, B. Pan, S.H. Lapidus, C. Liao, J.T. Vaughey, B.J. Ingram, Rechargeable ca-ion batteries: a new energy storage system, Chem. Mater. 27 (24) (2015) 8442–8447.

[3] S. Gheytani, Y. Liang, F. Wu, Y. Jing, H. Dong, K.K. Rao, X. Chi, F. Fang, Y. Yao, An aqueous ca-ion battery, Adv. Sci. 4 (12) (2017) 1700465.

[4] Y. Liang, H. Dong, D. Aurbach, Y. Yao, Current status and future directions of multivalent metal-ion batteries, Nat. Energy 5 (9) (2020) 646–656.

[5] Z. Zhao-Karger, Y. Xiu, Z. Li, A. Reupert, T. Smok, M. Fichtner, Calcium-tin alloys as anodes for rechargeable non-aqueous calcium-ion batteries at room temperature, Nat. Commun. 13 (1) (2022) 3849.

[6] M.E. Arroyo-de Dompablo, A. Ponrouch, P. Johansson, M.R. Palacín, Achievements, challenges, and prospects of calcium batteries, Chem. Rev. 120 (14) (2019) 6331–6357.

[7] N. Kuperman, P. Padigi, G. Goncher, D. Evans, J. Thiebes, R. Solanki, High performance prussian blue cathode for nonaqueous ca-ion intercalation battery, J. Power Sources 342 (2017) 414–418.

[8] A. Shyamsunder, L.E. Blanc, A. Assoud, L.F. Nazar, Reversible calcium plating and stripping at room temperature using a borate salt, ACS Energy Lett. 4 (9) (2019) 2271–2276.

[9] Z. Li, O. Fuhr, M. Fichtner, Z. Zhao-Karger, Towards stable and efficient electrolytes for room-temperature rechargeable calcium batteries, Energy Environ. Sci. 12 (12) (2019) 3496–3501.

[10] M. Hayashi, H. Arai, H. Ohtsuka, Y. Sakurai, Electrochemical characteristics of calcium in organic electrolyte solutions and vanadium oxides as calcium hosts, J. Power Sources 119–121 (2003) 617–620, https://doi.org/10.1016/S0378-7753(03)00307-0. URL, https://www.sciencedirect.com/science/article/pii/S0378775303003070.

[11] D. Aurbach, R. Skaletsky, Y. Gofer, The electrochemical behavior of calcium electrodes in a few organic electrolytes, J. Electrochem. Soc. 138 (12) (1991) 3536.

[12] Z. Yao, V.I. Hegde, A. Aspuru-Guzik, C. Wolverton, Discovery of calcium-metal alloy anodes for reversible ca-ion batteries, Adv. Energy Mater. 9 (9) (2019) 1802994.

[13] A. Ponrouch, D. Tchitchekova, C. Frontera, F. Bardé, M.E. Arroyo-de Dompablo, M.R. Palacín, Assessing si-based anodes for ca-ion batteries: electrochemical decalciation of casi2, Electrochem. Commun. 66 (2016) 75–78.

[14] I.V. Chepkasov, M. Ghorbani-Asl, Z.I. Popov, J.H. Smet, A.V. Krasheninnikov, Alkali metals inside bi-layer graphene and mos2: insights from first-principles calculations, Nano Energy 75 (2020) 104927, https://doi.org/10.1016/j.nanoen.2020.104927.

[15] M. Kühne, F. Börrnert, S. Fecher, M. Ghorbani-Asl, J. Biskupek, D. Samuelis, A.V. Krasheninnikov, U. Kaiser, J.H. Smet, Reversible superdense ordering of lithium between two graphene sheets, Nature 564 (7735) (2018) 234–239, https://doi.org/10.1038/s41586-018-0754-2.

[16] I.V. Chepkasov, J.H. Smet, A.V. Krasheninnikov, Single-and multilayers of alkali metal atoms inside graphene/mos2 heterostructures: a systematic first-principles study, J. Phys. Chem. C 126 (37) (2022) 15558–15564, https://doi.org/10.1021/acs.jpcc.2c03749.

[17] X. Zhang, M. Ghorbani-Asl, Y. Zhang, A.V. Krasheninnikov, Quasi-2d fcc lithium crystals inside defective bi-layer graphene: insights from first-principles calculations, Mater. Today Energy 34 (2023) 101293.

[18] N. Emery, C. Hérold, P. Lagrange, Structural study and crystal chemistry of the first stage calcium graphite intercalation compound, J. Solid State Chem. 178 (9) (2005) 2947–2952.

[19] B. Mortazavi, A. Dianat, O. Rahaman, G. Cuniberti, T. Rabczuk, Borophene as an anode material for ca, mg, na or li ion storage: a first-principle study, J. Power Sources 329 (2016) 456–461.

[20] A.H.F. Niaei, T. Hussain, M. Hankel, D.J. Searles, Hydrogenated defective graphene as an anode material for sodium and calcium ion batteries: a density functional theory study, Carbon 136 (2018) 73–84.

[21] D. Kong, T. Cai, H. Fan, H. Hu, X. Wang, Y. Cui, D. Wang, Y. Wang, H. Hu, M. Wu, et al., Polycyclic aromatic hydrocarbons as a new class of promising cathode materials for aluminum-ion batteries, Angew. Chem. Int. Ed. 61 (3) (2022) e202114681.

[22] J.H. Park, T. Liu, K.C. Kim, S.W. Lee, S.S. Jang, Systematic molecular design of ketone derivatives of aromatic molecules for lithium-ion batteries: first-principles dft modeling, ChemSusChem 10 (7) (2017) 1584–1591.

[23] P.K. Ramya, C.H. Suresh, Polycyclic aromatic hydrocarbons as anode materials in lithium-ion batteries: a dft study, J. Phys. Chem. 127 (11) (2023) 2511–2522, https://doi.org/10.1021/acs.jpca.3c00337.

[24] S. Panigrahi, G.N. Sastry, Reducing polyaromatic hydrocarbons: the capability and capacity of lithium, RSC Adv. 4 (28) (2014) 14557–14563.

[25] D. Vijay, G.N. Sastry, Exploring the size dependence of cyclic and acyclic π-systems on cation–π binding, Phys. Chem. Chem. Phys. 10 (4) (2008) 582–590.

[26] S. Ishikawa, G. Madjarova, T. Yamabe, First-principles study of the lithium interaction with polycyclic aromatic hydrocarbons, J. Phys. Chem. B 105 (48) (2001) 11986–11993.

[27] T.A. Baker, M. Head-Gordon, Modeling the charge transfer between alkali metals and polycyclic aromatic hydrocarbons using electronic structure methods, J. Phys. Chem. 114 (37) (2010) 10326–10333.

[28] R. Friedlein, X. Crispin, W.R. Salaneck, Molecular parameters controlling the energy storage capability of lithium polyaromatic hydrocarbon intercalation compounds, J. Power Sources 129 (1) (2004) 29–33.

[29] G. Kresse, J. Furthmüller, Efficient iterative schemes for ab initio total-energy calculations using a plane-wave basis set, Phys. Rev. B 54 (16) (1996) 11169.

[30] G. Kresse, D. Joubert, From ultrasoft pseudopotentials to the projector augmented-wave method, Phys. Rev. B 59 (3) (1999) 1758.

[31] H.J. Monkhorst, J.D. Pack, Special points for brillouin-zone integrations, Phys. Rev. B 13 (12) (1976) 5188.

[32] S. Grimme, J. Antony, S. Ehrlich, H. Krieg, A consistent and accurate ab initio parametrization of density functional dispersion correction (dft-d) for the 94 elements h-pu, J. Chem. Phys. 132 (15) (2010) 154104.

[33] Z.M. Abardeh, A. Salimi, A.R. Oganov, Crystal structure prediction of n-halide phthalimide compounds: halogen bonding synthons as a touchstone, CrystEngComm 24 (34) (2022) 6066–6075.

[34] W. Tang, E. Sanville, G. Henkelman, A grid-based bader analysis algorithm without lattice bias, J. Phys. Condens. Matter 21 (8) (2009) 084204.

[35] S.P. Ong, W.D. Richards, A. Jain, G. Hautier, M. Kocher, S. Cholia, D. Gunter, V.L. Chevrier, K.A. Persson, G. Ceder, Python materials genomics (pymatgen): a robust, open-source python library for materials analysis, Comput. Mater. Sci. 68 (2013) 314–319.

[36] K. Momma, F. Izumi, Vesta: a three-dimensional visualization system for electronic and structural analysis, J. Appl. Crystallogr. 41 (3) (2008) 653–658.

[37] G. Henkelman, B.P. Uberuaga, H. Jónsson, A climbing image nudged elastic band method for finding saddle points and minimum energy paths, J. Chem. Phys. 113 (22) (2000) 9901–9904, https://doi.org/10.1063/1.1329672.

[38] C.P. Brock, J. Dunitz, Temperature dependence of thermal motion in crystalline anthracene, Acta Crystallogr. Sect. B Struct. Sci. 46 (6) (1990) 795–806.

[39] D. Holmes, S. Kumaraswamy, A.J. Matzger, K.P.C. Vollhardt, On the nature of nonplanarity in the [n] phenylenes, Chem. Eur. J. 5 (11) (1999) 3399–3412.

[40] C. Tayran, S. Aydin, M. Cakmak, Ş. Ellialtıoğlu, Structural and electronic properties of ab-and aa-stacking bilayer-graphene intercalated by li, na, ca, b, al, si, ge, ag, and au atoms, Solid State Commun. 231 (2016) 57–63.

[41] F.D. Romero, M. Pitcher, C. Hiley, G. Whitehead, S. Kar, A. Ganin, D. Antypov, C. Collins, M. Dyer, G. Klupp, et al., Redox-controlled potassium intercalation into two polyaromatic hydrocarbon solids, Nat. Chem. 9 (7) (2017) 644–652, https://doi.org/10.1038/nchem.2765.

[42] R. Mitsuhashi, Y. Suzuki, Y. Yamanari, H. Mitamura, T. Kambe, N. Ikeda, H. Okamoto, A. Fujiwara, M. Yamaji, N. Kawasaki, et al., Superconductivity in alkali-metal-doped picene, Nature 464 (7285) (2010) 76–79, https://doi.org/10.1038/nature08859.

[43] Q.T. Phan, S. Heguri, H. Tamura, T. Nakano, Y. Nozue, K. Tanigaki, Two different ground states in k-intercalated polyacenes, Phys. Rev. B 93 (7) (2016) 075130, https://doi.org/10.1103/PhysRevB.93.075130.

[44] K. Hummer, C. Ambrosch-Draxl, Electronic properties of oligoacenes from first principles, Phys. Rev. B 72 (20) (2005) 205205.

[45] I.V. Chepkasov, A.V. Krasheninnikov, Tetracene crystals as promising anode material for alkali metal ion batteries, Carbon (2023) 118190.

[46] Z.-L. Xu, J. Park, J. Wang, H. Moon, G. Yoon, J. Lim, Y.-J. Ko, S.-P. Cho, S.-Y. Lee, K. Kang, A new high-voltage calcium intercalation host for ultra-stable and high-power calcium rechargeable batteries, Nat. Commun. 12 (1) (2021) 3369.

[47] H. Park, Y. Cui, S. Kim, J. Vaughey, P. Zapol, Ca cobaltites as potential cathode materials for rechargeable ca-ion batteries: theory and experiment, J. Phys. Chem. C 124 (11) (2020) 5902–5909.

[48] J. Carrasco, Role of van der waals forces in thermodynamics and kinetics of layered transition metal oxide electrodes: alkali and alkaline-earth ion insertion into v2o5, J. Phys. Chem. C 118 (34) (2014) 19599–19607.

[49] M.E. Arroyo-de Dompablo, C. Krich, J. Nava-Avendaño, M.R. Palacín, F. Bardé, In quest of cathode materials for ca ion batteries: the camo 3 perovskites (m= mo, cr, mn, fe, co, and ni), Phys. Chem. Chem. Phys. 18 (29) (2016) 19966–19972.

[50] A. Torres, F. Luque, J. Tortajada, M. Arroyo-de Dompablo, Dft investigation of ca mobility in reduced-perovskite and oxidized-marokite oxides, Energy Storage Mater. 21 (2019) 354–360.